Brownian dynamics and kinetic glass transition in colloidal suspensions

Hartmut Löwen,* Jean-Pierre Hansen, and Jean-Noël Roux
Laboratoire de Physique, Ecole Normale Supérieure de Lyon, 69364 Lyon CEDEX 07, France
(Received 23 January 1991)

Structural slowing down in a simple model of a polydisperse suspension of charge-stabilized colloidal particles is explored by molecular-dynamics and Brownian-dynamics simulations. The former ignore solvent effects, but allow a comparison with recent experimental, numerical, and theoretical work on "fragile" glass formers. Solvent friction is taken care of in the irreversible Brownian-dynamics simulations, but solvent-induced hydrodynamic interactions between colloidal particles are neglected. Self-diffusion is found to proceed by hopping processes, near and below the kinetic glass transition temperature, even in the case of Brownian dynamics, where cooperative phonon processes are overdamped. Newtonian and Brownian dynamics lead to qualitatively different relaxations of the density fluctuations. The density autocorrelation functions calculated with Brownian equations of motion show no evidence of β relaxation. The simulation results are discussed in the light of recent dynamic-light-scattering experiments on concentrated colloidal suspensions.

I. INTRODUCTION

It is by now well established, both experimentally and theoretically, that suspensions of colloidal particles in water or nonaqueous solvents exhibit a local structure and a phase behavior which are highly reminiscent of those observed in simple atomic systems [1]. Colloidal crystals, strikingly visualized by Bragg reflection of visible light, have been the object of intense investigations over the past two decades [2], and more recent experiments have shown that highly concentrated suspensions of sterically stabilized colloidal particles exhibit both crystalline and amorphous solid phases [3]. Extensive dynamic-light-scattering measurements [4] have revealed that the transition from the colloidal liquid to the glass is signaled by a characteristic "structural arrest" in the long-time decay of density fluctuations, very similar to the behavior predicted by mode-coupling theory [5] of the kinetic glass transition, and observed by inelastic neutron-scattering experiments on simple atomic systems [6]. Now it is well known that, due to the presence of the solvent, the short-time dynamics of the colloidal particles are governed by equations of motion very different from the Newtonian dynamics of atomic systems. On the time scale between two successive collisions with other colloidal particles, a given particle will undergo Brownian, rather than free-particle (ballistic) motion. Consequently the irreversible time evolution of any dynamical variable associated with the mesoscopic colloidal particles will be governed by the Smoluchowski, rather than by the Liouville operator [1].

The main objective of the present work is to investigate the influence of these very different time evolutions on structural relaxation in a simple model of colloidal suspensions. To this purpose we have carried out extensive numerical simulations of the model, using both molecular (or Newtonian) dynamics (MD) [7] and Brownian dynamics (BD) [8,7] to explore its single-particle and collective dynamical behavior for several temperatures.

The paper is organized as follows. Our model for a charge-stabilized colloidal suspension is introduced in Sec. II. The two basic time evolutions are presented in Sec. III, together with the relevant numerical algorithms. Static properties are briefly summarized in Sec. IV, while the simulation results for the single-particle motion (self-diffusion) are presented in Sec. V. Section VI contains the key results on the decay of density fluctuations, and the qualitative differences between the data obtained with Brownian and Newtonian dynamics are discussed in Sec. VII, by comparison with the dynamic-light-scattering experiments of van Megen and Pusey [4].

II. MODEL

To model a charge-stabilized colloidal suspension, we have chosen a polydisperse system of particles interacting via purely repulsive Yukawa potentials [9], namely,

$$v_{ij}(r)=U_0\frac{a}{r}\frac{Z_iZ_j}{\bar{Z}^2}\exp\left[-\kappa\frac{r-a}{a}\right]\equiv U_0\tilde{Z}_i\tilde{Z}_j\phi(r)\ , \quad (1)$$

where U_0 is the energy scale, a is the length scale, Z_i is the valence of particle i, $\bar{Z}$ the mean valence, and $\tilde{Z}_i=Z_i/\bar{Z}$ the normalized valence. κ is the reduced inverse screening length due to the counterions and added salt. The valences Z are assumed to be distributed according to a Schultz distribution:

$$P(Z)=\frac{1}{\bar{Z}}\frac{(\nu+1)^{\nu+1}}{\Gamma(\nu+1)}\left[\frac{Z}{\bar{Z}}\right]^{\nu}\exp\left[-(\nu+1)\frac{Z}{\bar{Z}}\right]\ , \quad (2)$$

which is characterized by two parameters, namely, the mean valence

$$\bar{Z}=\int_0^\infty P(Z)Z\,dZ \quad (3)$$

and the exponent ν which controls the relative polydispersity

$$p_Z=\frac{1}{\bar{Z}}\left[\int_0^\infty P(Z)(Z-\bar{Z})^2dZ\right]^{1/2}. \quad (4)$$

Charge (or size) polydispersity is an intrinsic feature of real colloidal suspensions. But our main reason for considering a polydisperse suspension, rather than the simpler monodisperse system, is that, due to size-mismatch frustration, polydispersity inhibits nucleation, and thus allows one to bypass spontaneous crystallization of the samples within the duration of the simulations. For similar reasons, earlier simulations of the glass transition in atomic systems were performed on simple binary-alloy models [10].

Crystallization of the monodisperse version of the Yukawa model ($p_Z=0$) has been investigated by the extensive MD simulations of Robbins, Kremer, and Grest [11], for a wide range of screening parameters κ. Their results provide a useful guide for estimating the temperature or density range where the polydisperse colloidal liquid may be expected to undergo a glass transition towards an amorphous solid. The simulations reported below were all carried out for the value $\kappa=7$ of the screening parameter; this amounts to a regime of strong screening and the corresponding "effective" monodisperse system, with a valence equal to $\bar{Z}$, crystallizes into an fcc lattice at a reduced temperature $T^*=k_BT/U_0\simeq 0.57$ [11]. Consequently we carried out MD and BD simulations in the range $0.10\le T^*\le 0.45$, for a fixed number density $\rho=N/V=a^{-3}$. Thus a corresponds to a typical interparticle spacing. The simulation cell of volume V contained $N=500$ particles, with valences Z_i evenly distributed according to the Schultz distribution (2) as follows: $N+1$ grid points $\{Z_j^G\}$ were chosen by solving

$$\int_{Z_j^G}^{Z_{j+1}^G} P(Z)dZ=1/N,\quad 1\le j\le N$$

with $Z_1^G=0$, $Z_{N+1}^G=\infty$ and the N charges were then determined by

$$Z_j=N\int_{Z_j^G}^{Z_{j+1}^G} ZP(Z)dZ\ . \quad (5)$$

The resulting distribution of charges is shown in Fig. 1, for a value of the relative polydispersity $p_Z=0.5$, which was adopted throughout in the simulations reported below. As shown in Ref. [9], the charge polydisperse Yukawa fluid may be mapped onto an effective polydisperse hard-sphere reference system via the Gibbs-Bogoliubov inequality. With the present choice $\kappa=7$ and $p_Z=0.5$, the resulting effective size polydispersity of the hard-sphere reference system turns out to be $p_\sigma=0.13$, for the thermodynamic state $T^*=0.14$ and $\rho=a^{-3}$; $p_\sigma=0.13$ is typically of the order of the size polydispersity needed to destabilize the chemically disordered fcc-crystal, thus favoring the formation of an amorphous solid [12].

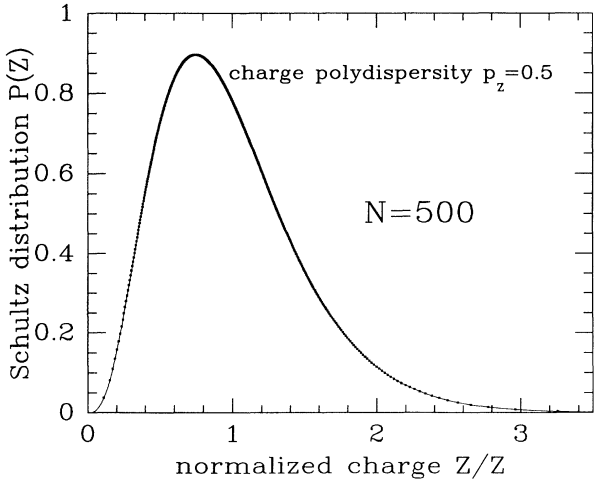

FIG. 1. Schultz distribution of charges [Eq. (2)] vs $Z/\bar{Z}$, for the relative polydispersity $p_Z=0.5$ used in the present work.

III. NEWTONIAN VERSUS BROWNIAN DYNAMICS

We have mapped out phase-space trajectories of the model defined in the preceding section, using finite difference versions of both Newtonian (MD) and Brownian (BD) equations of motion. The total force exerted on particle i by the $N-1$ other particles derives from the potentials (1):

$$\mathbf{F}_i=-\nabla_i V_N=-U_0\sum_{j\neq i}\tilde{Z}_i\tilde{Z}_j\nabla_i\phi(|\mathbf{r}_i-\mathbf{r}_j|)\ . \quad (6)$$

In the absence of solvent, Newton's equations of motion hold, so that the positions of the particles evolve according to the N coupled second-order differential equations:

$$m\ddot{\mathbf{r}}_i(t)=\mathbf{F}_i(\{\mathbf{r}_j(t)\})\ , \quad (7)$$

where the masses of all particles have been taken to be equal. The natural time scale associated with the Newtonian equations (7) is $\tau_N=(ma^2/U_0)^{1/2}$. We have integrated the equations of motion (7) using the standard Verlet algorithm and a constant temperature constraint [7], with a time step $\Delta t=0.008\tau_N$. This part of our simulations is rather similar to some recent work on the glass transition in monodisperse and binary colloidal systems, assuming Newton's equations of motion, which ignore the solvent [13].

In the presence of a solvent, the colloidal particles undergo frequent random collisions with the solvent molecules which lead to Brownian motion on time scales $t>\tau_0=m/\xi$ governed by the macroscopic friction coefficient ξ. The resulting, irreversible coupled equations of motion read [1,7]

$$\xi\dot{\mathbf{r}}_i(t)=\mathbf{F}_i(t)+\mathbf{R}(t)\ , \quad (8)$$

where $\mathbf{R}$ denotes the Langevin random force. The natural time scale associated with the Brownian equations of motion is $\tau_B=\xi a^2/U_0=k_BTa^2/(U_0D_0)$, where $D_0=k_BT/\xi$ denotes the short-time diffusion coefficient. Finite difference integration of Eq. (8) leads to the BD algorithm [8,7]

$$\mathbf{r}_i(t+\Delta t)=\mathbf{r}_i(t)+\frac{1}{\xi}\mathbf{F}_i(t)\Delta t+(\Delta\mathbf{r})_R+O((\Delta t)^2)\ , \tag{9}$$

where the random displacement $(\Delta\mathbf{r})_R$ is sampled from a Gaussian distribution of zero mean and variance $\langle(\Delta\mathbf{r})_R^2\rangle=6D_0\Delta t$. Due to the random nature of the dynamics, embodied in $(\Delta\mathbf{r})_R$, the velocities of the colloidal particles are undefined; the temperature, which is related to the kinetic energy when Newtonian dynamics are used, determines the variance $6D_0\Delta t=6k_BT\Delta t/\xi$ in the case of Brownian dynamics, where we make the additional assumption that the friction coefficient ξ is a constant (conveniently taken to be 1), independent of temperature, thus determining the time scale. The variance $\langle(\Delta\mathbf{r})_R^2\rangle$ is hence linearly related to T and serves as input in BD runs. Note that the error made with the algorithm (9) is $O((\Delta t)^2)$, compared to an error $O((\Delta t)^4)$ in the Verlet algorithm for Newtonian dynamics. Consequently, the time step Δt must be chosen to be smaller in order to ensure a reasonable stability of the trajectories; we found $\Delta t\simeq 0.003\tau_B$ to be a satisfactory choice. BD simulations of the type just described have been used earlier [14] to investigate fluidlike states of colloidal suspensions in the low concentration and weak screening regime. Due to the random contribution to the displacements in the equations of motion (9), the center of mass of the total system must be held fixed in order to avoid any spurious relaxation of the correlation functions at long times.

The Brownian equation of motion (8) accounts for solvent friction, but ignores hydrodynamic interactions between colloidal particles due to the velocity field set up in the solvent by the moving colloidal particles. The effect of these hydrodynamic interactions is to replace the scalar single-particle diffusion constant D_0 by a configuration-dependent $3N\times 3N$ diffusion tensor $\vec{\mathbf{D}}(\{\mathbf{r}_j\})$. Neglect of the hydrodynamic interactions is certainly not justified at high concentrations, but their inclusion would represent a formidable theoretical and numerical task, which is far from being solved. However, since the investigation of the long-time behavior of correlation functions near the glass transition, which is the primary objective of the present work, requires the simplest possible algorithm, to allow for long phase-space trajectories, we have chosen to ignore hydrodynamic interactions altogether, and to focus on the BD *model*, embodied in the equation of motion (9); the latter has at least the merit of having the same general irreversible structure as in the much more complex case where hydrodynamic interactions are included.

The time evolution of any dynamical variable $A(t)$ is determined by the Liouville and adjoint Smoluchowski operators for Newtonain and Brownian dynamics, respectively, i.e.,

$$A(t)=\exp(\mathcal{L}t)A(0)\ , \tag{10}$$

$$\mathcal{L}=\sum_{j=1}^{N}\left[\frac{d\mathbf{r}_j}{dt}\cdot\frac{\partial}{\partial\mathbf{r}_j}+\frac{d\mathbf{p}_j}{dt}\cdot\frac{\partial}{\partial\mathbf{p}_j}\right]$$

(Newtonian dynamics) ,

TABLE I. Cooling history of the different runs. Also given are the number of equilibration time steps N_{eq}, the number of production time steps N_t, the time step Δt^* in reduced units, as well as the temperature T^*, the reduced equation of state $Z^*=p/(\rho k_BT)$ and the diffusion coefficient D^*. The density is constant $\rho=a^{-3}$. MD or BD indicates whether molecular or Brownian dynamics was used. The starting positions are also given, where the velocities are scaled to get the new temperature (for MD).

Run	MD or BD	N_{eq}	N_t	Δt^*	T^*	Z^*	$D^*\times 10^3$	Starting position
a01	MD	7000	5000	0.008	0.455	19.5		fcc
a02	MD	25000	25000	0.008	0.349	24.5		a01
a03	MD	10000	10000	0.008	0.240	33.5	12.7	a02
a04	MD	10000	10000	0.008	0.200	39.5	8.2	a03
a05	MD	8000	10000	0.008	0.180	43.4	5.4	a04
a06	MD	50000	30000	0.008	0.157	49.2	3.0	a05
a07	MD	100000	60000	0.008	0.151	51.0	2.3	a06
a08	MD	50000	50000	0.008	0.141	54.4	1.5	a07
a09	MD	50000	50000	0.008	0.134	57.0	1.0	a08
a10	MD	80000	100000	0.008	0.127	59.9	0.66	a09
a11	MD	100000	100000	0.008	0.120	63.2	0.39	a10
a12	MD	100000	100000	0.008	0.110	69.1	0.19	a11
a13	MD	100000	100000	0.008	0.100	75.1	0.085	a12
a14	MD	100000	100000	0.008	0.115	65.8	0.23	a12
b01	BD	250000	200000	0.0040	0.110	69.5	0.1	a11
b02	BD	100000	200000	0.0035	0.115	66.1	0.3	b01
b03	BD	100000	200000	0.0035	0.120	63.5	0.6	b02
b04	BD	100000	200000	0.0035	0.130	58.9	1.2	b03
b05	BD	100000	200000	0.0034	0.140	54.9	2.3	b04
b06	BD	60000	80000	0.0030	0.150	51.5	3.9	b05
b07	BD	100000	200000	0.0040	0.100	75.5	0.09	b01

$$A(t)=\exp(\tilde{\mathcal{O}}t)A(0)\ ,$$
$$\tilde{\mathcal{O}}=\sum_{j=1}^{N} D_0\left[-\beta\frac{\partial V_N}{\partial \mathbf{r}_j}+\frac{\partial}{\partial \mathbf{r}_j}\right]\cdot\frac{\partial}{\partial \mathbf{r}_j} \quad \text{(Brownian dynamics)}\ . \tag{11}$$

In Eq. (10), $\mathbf{p}_j$ denotes the momentum of particle j; due to the coarse graining ($\tau_B \gg \tau_0$), momentum variables are absent in the Brownian (Smoluchowski) dynamics.

In view of the Hermitian nature of the Liouville operator, the time autocorrelation functions derived from Newtonian dynamics are even functions of time (i.e., they are invariant under time reversal), whereas the autocorrelation functions derived from the Smoluchowski propagator are not time reversible, and their short-time expansions exhibit both odd and even powers of t. This simple remark will have important consequences in Sec. VII.

Table I lists the characteristics of the various runs which we carried out, using MD or BD. Starting from the highest temperature ($T^*=0.45$), the system was slowly cooled down to $T^*=0.10$. Especially at the lower temperatures, where the glass transition is expected to take place, the cooling rate was very gentle, with long equilibration runs lasting of the order of 10^5 time steps, between successive temperatures. Production runs lasted from 10^5 to 2×10^5 time steps.

IV. STATIC PROPERTIES

For a given thermodynamic state and a given set of pair potentials (1), the static (or equal-time) correlation functions and the thermodynamic properties must be independent of the nature of the dynamics (MD or BD). Satisfaction of this requirement provides a good consistency test of the simulations.

The basic static quantities which were systematically computed are the averaged and charge-averaged pair distribution functions:

$$g(r)=\frac{1}{\rho N}\left\langle\sum_{i\neq j}\delta(\mathbf{r}-\mathbf{r}_i+\mathbf{r}_j)\right\rangle\ , \tag{12a}$$

$$g_Z(r)=\frac{1}{\rho N}\left\langle\sum_{i\neq j}\tilde{Z}_i\tilde{Z}_j\delta(\mathbf{r}-\mathbf{r}_i+\mathbf{r}_j)\right\rangle\ . \tag{12b}$$

The latter yields directly the (osmotic) pressure according to the virial theorem for a charge-polydisperse system:

$$\frac{p}{\rho k_B T}=1-\frac{2\pi}{3}\frac{\rho U_0}{k_B T}\int_0^\infty g_Z(r)\frac{d\phi(r)}{dr}r^3dr\ . \tag{13}$$

Examples of $g(r)$ and $g_Z(r)$ (for a rectangular, rather than Schultz distribution of charges) are shown in Ref. [9]. Equation-of-state data are given in Table I; for a fixed value of the density ($\rho=1/a^3$), $p/(\rho k_B T)$ turns out to be practically linear in $1/T$ over the whole temperature range explored by our simulations.

The Fourier transform of $g(r)$ yields the static structure factor $S(k)$. Our results for $T^*=0.15$ and 0.115 are shown in Fig. 2. The interesting feature is the splitting of the second peak at the lower temperature, which is probably the result of two slightly different spatial scales due to polydispersity. At the higher temperature, the splitting appears to be washed out. The same splitting is observed in the charge-averaged structure factor $S_Z(k)$, the Fourier transform of (12b). It may be worth pointing out that in monodisperse atomic systems, split second peaks in the pair distribution function, rather than in the structure factor, have often been considered as signaling the onset of glassy behavior. A similar splitting of the second peak in the structure factor has been found in a simulation of a supercooled metallic liquid [15].

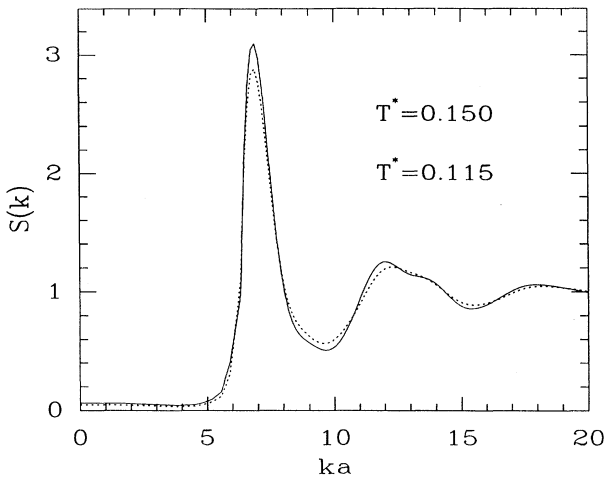

FIG. 2. Total structure factor $S(k)$ vs reduced wave number ka; dashed curve, $T^*=0.15$; solid curve, $T^*=0.115$.

Finally, as noted at the beginning of this section, we always observed that the differences between the static properties calculated for identical thermodynamic conditions by MD and BD agreed within statistical uncertainties. Also it may be of interest to note that our simulations never showed any indication of segregation of particles of different charges.

V. DIFFUSION

Approaching the glass transition is signaled by a rapid decrease of the (averaged) self-diffusion constant D of the colloidal particles. D is estimated from the slope of a plot of the mean-square displacement of the particles as a function of time (Einstein plot). In the Newtonian case, D may also be calculated by numerical integration of the velocity autocorrelation function. An example of the normalized velocity autocorrelation function is shown in Fig. 3, for a thermodynamic state in the supercooled fluid region ($T^*=0.15$); the qualitative behavior closely resembles the data published by Robbins, Kremer, and Grest [11] for the monodisperse Yukawa fluid. The force autocorrelation function

$$\mathcal{F}(t)=\langle\mathbf{F}(t)\cdot\mathbf{F}(0)\rangle=-m^2\frac{d^2}{dt^2}\langle\mathbf{v}(t)\cdot\mathbf{v}(0)\rangle \tag{14}$$

is also shown in Fig. 3, together with the corresponding

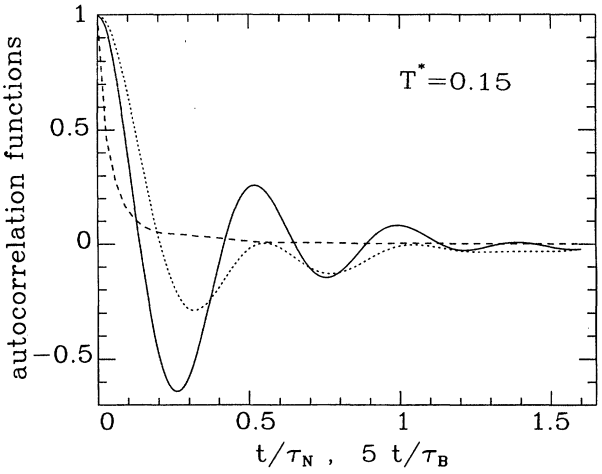

FIG. 3. Velocity and force autocorrelation functions vs reduced time, for $T^*=0.15$. The solid (force autocorrelation function) and dotted (velocity autocorrelation function) curves are for Newtonian dynamics (time in units of τ_N); the dashed curve represents the force autocorrelation function for Brownian dynamics (time in units of $\tau_B/5$).

function for the BD case for which the $\delta(t)$ contribution from the random force has been subtracted. The difference in short-time behavior between the Newtonian and Brownian dynamics is strikingly illustrated by this comparison.

Values of the reduced diffusion constants $D_N^*=D\tau_N/a^2$ and $D_B^*=D\tau_B/a^2$ from our MD and BD simulations are listed in Table I and plotted in Fig. 4. Plots of $\ln(D_N^*)$ [$\ln(D_B^*)$] versus $\ln(T^*-T_0^*)$ are reasonably linear for adequate choices of the "transition" temperature T_0^N [T_0^B], except at the lowest temperatures,

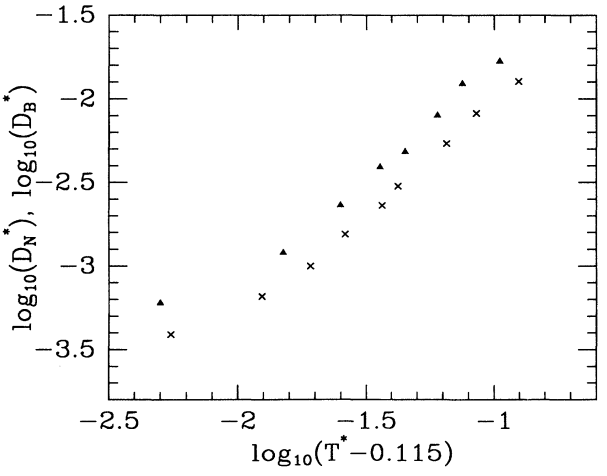

FIG. 4. Log-log plot of the reduced diffusion constants, $D_N^*=D_N\tau_N/a^2$ (Newtonian dynamics, crosses) and $D_B^*=D_B\tau_B/a^2$ (Brownian dynamics, triangles) vs reduced temperature $T^*-0.115$.

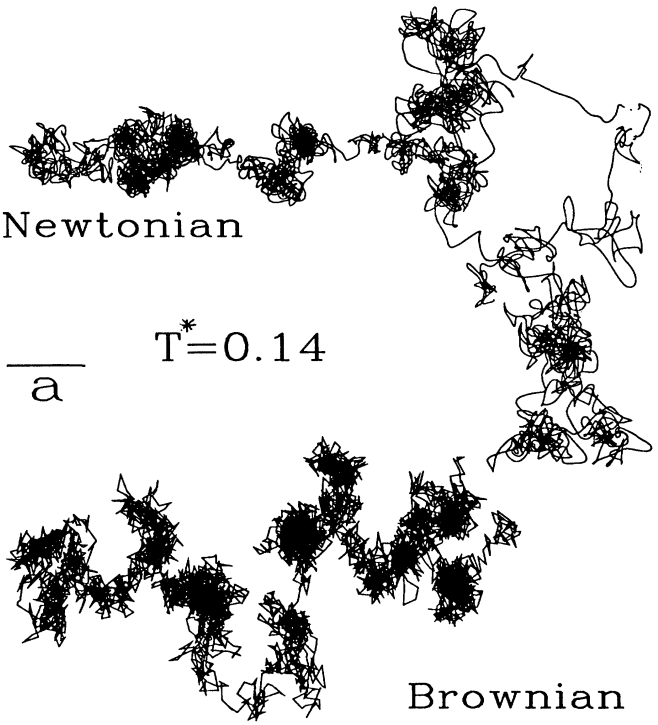

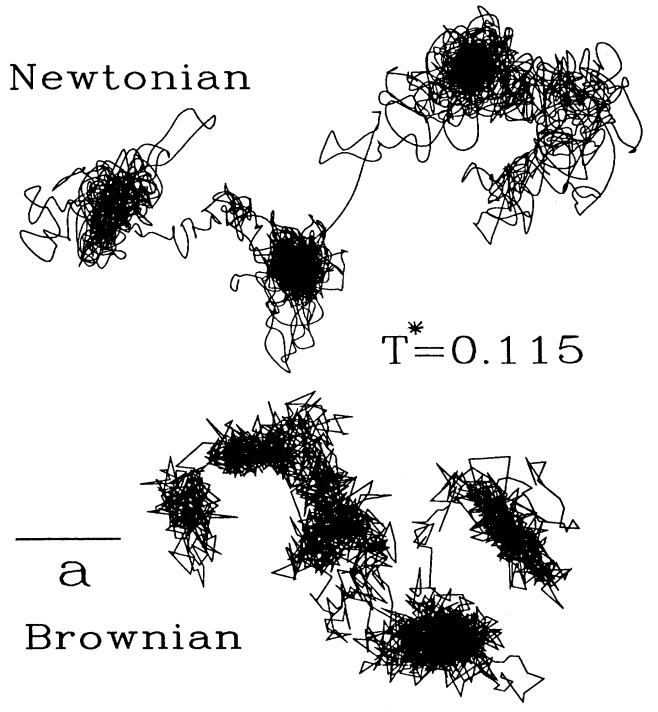

FIG. 5. Typical trajectories of one lightly charged particle, projected onto a plane; upper trajectories, Newtonian dynamics; lower trajectories, Brownian dynamics; (a) $T^*=0.14$; (b) $T^*=0.115$. The horizontal segment indicates the length scale a; trajectories cover 10^5 (2×10^5) time steps for Newtonian (Brownian) dynamics.

suggesting approximate power-law behavior of the form

$$D^* = A(T^* - T_0^*)^\gamma + \delta D^* , \tag{15}$$

where the small "residual" contribution δD^* may be attributed to activated processes, i.e., jump diffusion events within a frozen disordered structure. The measured exponent γ turns out to be of the order of $\gamma \simeq 1.4$, for both types of dynamics, with $T_0^{N*}, T_0^{B*} \simeq 0.12 \pm 0.01$. Note that the optimum value of the exponent γ is significantly smaller than the value $\gamma \simeq 2$ found in the binary-alloy case [10], thus confirming the nonuniversal nature of the scaling law predicted by mode-coupling theory [5]. It is noteworthy that mode-coupling theory predicts $\gamma \gtrsim 1.7$ for a simple one component system. Our low value of γ is due to polydispersity effects. The deviations from a power law in the vicinity of the glass transition are traditionally associated with activated jumps. This interpretation has been confirmed by a detailed analysis of the trajectories of the particles [16]. Projections of typical trajectories onto a plane, as generated in the course of both MD and BD simulations, are shown in Figs. 5(a) and 5(b), at temperatures just above and just below the estimated transition temperatures T_0^N and T_0^B. The change from diffusionlike to jump-controlled motion is clear-cut in the Newtonian case, as already observed in earlier simulations of binary alloys [10]; the observed change is not fundamentally different for Brownian dynamics, despite the lack of any collective "phonon assistance" which is conceivable only with Newtonian dynamics.

The qualitative change from diffusionlike to hopping-dominated single-particle motion may be characterized by the time dependence of the self-part, $G_S(r,t)$, of the Van Hove density-density correlation function, conveniently defined by

$$G_S(r,t) = \frac{1}{N}\left\langle \sum_{j=1}^{N} \delta(\mathbf{r} - \mathbf{r}_j(0) + \mathbf{r}_j(t)) \right\rangle . \tag{16}$$

As shown in Ref. [10], for the case of a binary-alloy model, $4\pi r^2 G_S(r,t)$ provides a rather clear-cut diagnostic

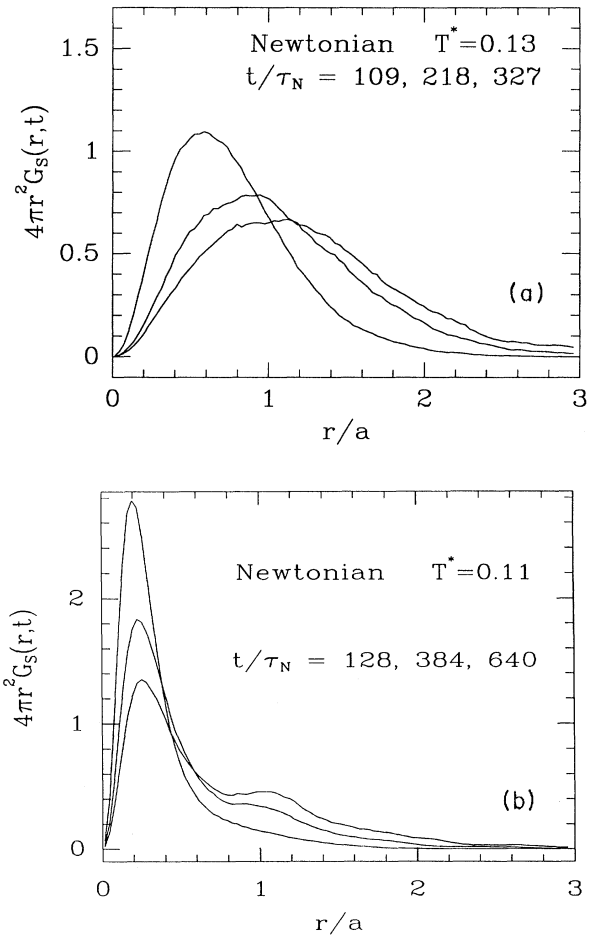

FIG. 6. Self-part of the Van Hove function, $G_S(r,t)$, multiplied by $4\pi r^2 a$ vs reduced distance r/a calculated with Newtonian dynamics; the curves from left to right (or top to bottom) are for increasing time arguments. (a) Results for $T^* = 0.13$ and $t^* = t/\tau_N = 109, 218, 327$. (b) Results for $T^* = 0.11$ and $t^* = 128, 384, 640$.

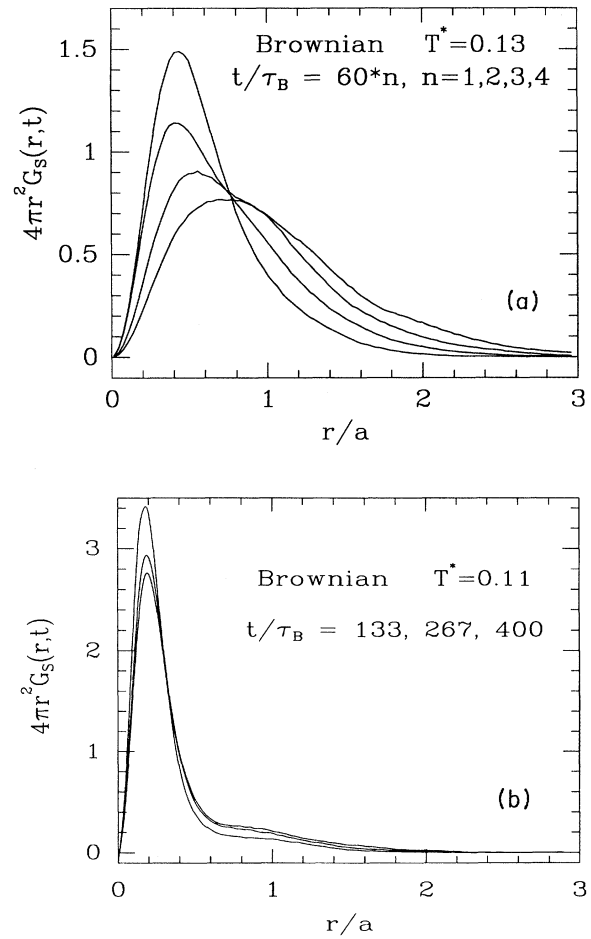

FIG. 7. Same as in Fig. 6, but for Brownian dynamics. (a) $T^* = 0.13$, $t^* = t/\tau_B = 60, 120, 180, 240$. (b) $T^* = 0.11$, $t^* = 133, 267, 400$.

for the kinetic glass transition, since it crosses over from a time-dependent shape very similar to that predicted by the macroscopic diffusion equation, to a behavior characteristic of a frozen structure over a narrow temperature interval, thus allowing a relatively unambiguous determination of the transition temperature T_0. Very much the same behavior is observed for the present polydisperse model, both with Newtonian and Brownian equations of motion; this is illustrated in Figs. 6(a), 6(b), 7(a), and 7(b). Below T_0 the frozen structure is clearly characterized by the arrested main peak, while hopping leads to the buildup of a secondary peak at the nearest-neighbor distance. This allows the following clear-cut estimates of the transition temperature, namely, $0.115 < T_0^{N*} \lesssim T_0^{B*} < 0.12$, the estimate for the Brownian dynamics being slightly higher than for Newtonian dynamics.

VI. LONG-TIME RELAXATION OF DENSITY FLUCTUATIONS

The **k**-space density autocorrelation function (or intermediate scattering function) is defined, as usual, by

$$F(k,t)=\frac{1}{N}<\rho_{\mathbf{k}}(t)\rho_{-\mathbf{k}}(0)> \ , \tag{17}$$

where $\rho_{\mathbf{k}}(t)$ denotes a Fourier component of the microscopic density:

$$\rho_{\mathbf{k}}(t)=\sum_{j=1}^{N}\exp[i\mathbf{k}\cdot\mathbf{r}_j(t)] \ . \tag{18}$$

The sum over particles in Eq. (18) is taken irrespective of their charge. The self-part of $F(k,t)$ may be extracted in the usual manner, according to

$$F_S(k,t)=\frac{1}{N}\sum_{j=1}^{N}\langle\exp\{i\mathbf{k}\cdot[\mathbf{r}_j(t)-\mathbf{r}_j(0)]\}\rangle \ . \tag{19}$$

Note that in a polydisperse system, all terms in the sum on the right-hand side of Eq. (19) are different; $F_S(k,t)$ is the spatial Fourier transform of the Van Hove function $G_S(r,t)$ which was considered in the preceding section.

Structural relaxation may be conveniently characterized by examining the time dependence of the intermediate scattering function, for wave numbers k in the vicinity of the main peak of the static structure factor, i.e., for $k\simeq k_0\simeq 7.4/a$. In that range of wave numbers, collective modes associated with the conserved (hydrodynamic) variables are fully damped, so that density fluctuations are dominated by single-particle motion, and hence $F(k,t)$ is expected to be close to $F_S(k,t)$. In numerical simulations, a much better statistical accuracy is achieved for the latter function, because of the additional averaging over the contributions from the N particles. For that reason, we first focus on the time dependence of $F_S(k,t)$. To enhance the statistics, averages were taken over 300 wave vectors **k** compatible with the periodic boundary conditions, of modulus $k=|\mathbf{k}|$ in the range $7.2\le ak\le 7.6$. The results for four different temperatures in the vicinity of the estimated transition temperatures T_0^N and T_0^B, are shown in Fig. 8 for Newtonian dynamics, and in Fig. 9 for Brownian dynamics with a logarithmic abscissa covering nearly five decades in time. The difference in qualitative behavior is clearly apparent. At short times, the reversible Newtonian dynamics lead to a quadratic behavior, up to $t\simeq 0.1\tau_N$. For longer times the shape of the Newtonian $F_S(k,t)$ is very sensitive to temperature; the relaxation clearly proceeds in two steps, which may be tentatively identified with β relaxation, for times $t\lesssim\tau_N$, and α relaxation at much larger times. The two regimes are separated by a roughly horizontal plateau extending over a time interval which increases rapidly as the temperature drops below T_0^N. This general behavior is quite similar to that observed in

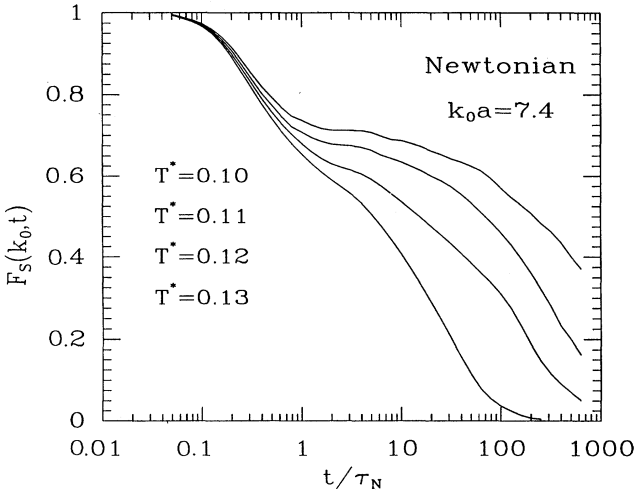

FIG. 8. Self-part of the density autocorrelation function $F_S(k,t)$ vs reduced time $t^*=t/\tau_N$ (on a logarithmic scale) for $k=k_0=7.4/a$ and (from bottom to top) $T^*=0.13$, 0.12, 0.11, and 0.10 (Newtonian dynamics).

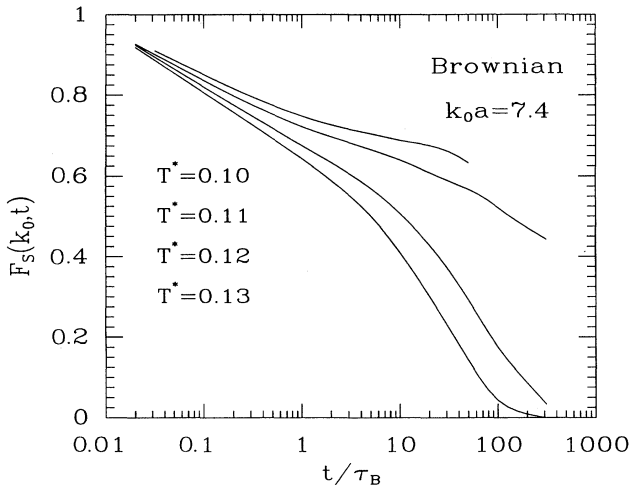

FIG. 9. $F_S(k,t)$ vs $t^*=t/\tau_B$ (on a logarithmic scale) for $k=k_0=7.4/a$ and (from bottom to top) $T^*=0.13$, 0.12, 0.11, and 0.10 (Brownian dynamics).

earlier simulations of atomic systems [10,17], and in inelastic neutron-scattering experiments [6]; it also agrees qualitatively with the predictions of mode-coupling theory, at least above the kinetic glass transition. The distinction between these two relaxation processes is clear in the frequency domain where they are associated with peaks at low and intermediate frequencies in the time-Fourier-transform of $F_S(k,t)$; see also [5] for a definition of α and β relaxation.

By contrast, the simulation data based on Brownian dynamics show the buildup of a plateau, characteristic of transient structural arrest, only at temperatures below T_0^{B*}. The curves change smoothly with decreasing T, but exhibit a strong enhancement of the rate of relaxation at long times, which may tentatively be identified with α relaxation.

Above the glass transition temperature T_0^N or T_0^B, the long-time decay of $F_S(k,t)$ is well fitted by a Kohlrausch stretched-exponential function:

$$F_S(k,t)=A\exp[-(t/t_0)^{\nu}] \ . \tag{20}$$

Typical values of the parameters a, t_0, and ν are listed in Table II. Note that the Kohlrausch exponent ν is larger for Brownian dynamics, compared to the Newtonian case.

The difference between the Newtonian and Brownian relaxational behaviors is strikingly revealed by examining the imaginary part of the susceptibility χ_S associated with $F_S(k,t)$. According to the fluctuation-dissipation theorem

$$\chi_S''(k,\omega)=\omega S_S(k,\omega) \ , \tag{21}$$

where $S_S(k,\omega)$ is the self-part of the dynamical structure factor which is easily calculated by numerical Fourier transformation of $F_S(k,t)$:

$$S_S(k,\omega)=\frac{1}{\pi}\int_0^{\infty}F_S(k,t)\cos(\omega t)dt \ . \tag{22}$$

χ_S'' is plotted in Fig. 10 as a function of frequency in the immediate vicinity of the glass transition. Putting aside the high-frequency contribution, arising from phonons and free particle motion, the spectrum calculated from Newtonian dynamics exhibits a well-defined low-frequency peak, which may be associated with α relaxation, as well as a pronounced shoulder at intermediate frequencies ($1\lesssim\omega\tau_N\lesssim 10$), which we interpret as being the signature of β relaxation; the two features are separated by a minimum in the spectrum, in agreement with theoretical predictions [5] and experimental observations [6]. The low- and intermediate-frequency ($\omega\tau_N\lesssim 10$) part of the spectrum is shifted to significantly lower frequencies at lower temperatures.

TABLE II. Parameters of the Kohlrausch fit: $\simeq A\exp[-(t/t_0)^{\nu}]$, for large t. The temperature is $T^*=0.13$.

Fitted Function	Dynamics	k_0	A	t_0	ν
$F_S(k_0,t)$	Newtonian	7.4	0.70	23.2	0.75
$F_S(k_0,t)$	Brownian	7.4	0.56	27.6	0.87
$\Phi(k_0,t)$	Newtonian	4.9	0.25	14.8	0.41
$\Phi(k_0,t)$	Brownian	4.9	0.01	17.0	0.73

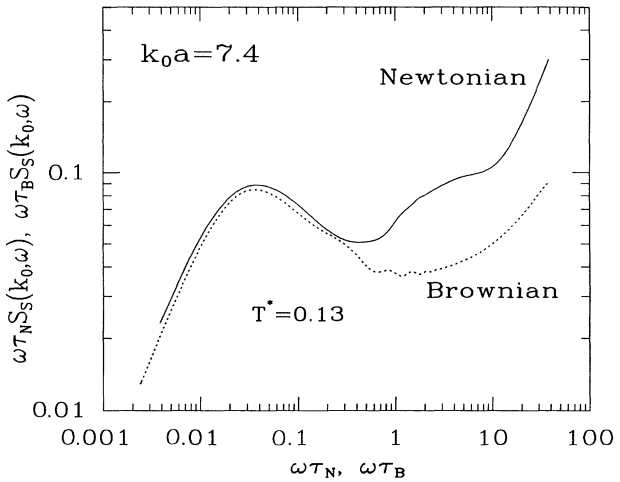

FIG. 10. Imaginary part of the self-response function $\chi_S''(k,\omega)=\omega\tau S_S(k,\omega)$ vs reduced frequency $\omega\tau$ (on a logarithmic scale) for $T^*=0.13$. Solid curve, Newtonian dynamics ($\tau=\tau_N$); dotted curve, Brownian dynamics ($\tau=\tau_B$).

Considering next the corresponding spectra obtained form the Brownian-dynamics simulations, it is immediately clear from Fig. 10 that the structure at intermediate frequencies observed in the Newtonian case is now completely absent. The Brownian spectrum reduces to a well-defined low-frequency α resonance separated from the high-frequency component due to free diffusion and damped phonons by a deep minimum, without any trace of a β-relaxation resonance.

As mentioned at the beginning of this section, the full density autocorrelation function $F(k,t)$ is not expected to differ significantly from its self-part $F_S(k,t)$ for $k\gtrsim k_0$. An example of the normalized function

$$\Phi(k,t)=\frac{F(k,t)}{F(k,t=0)}=\frac{F(k,t)}{S(k)} \tag{23}$$

is shown in Fig. 11, for both types of dynamics, and $k=k_0=7.4/a$. The two curves may be compared to their homologs in Figs. 8 and 9. The qualitative difference between Newtonian and Brownian dynamics is again clearly apparent: the incipient plateau in the Newtonian case is signaled by a change from positive to negative curvature around $t\simeq 2\tau_N$, while no such feature is visible for the Brownian correlation function. The inset of Fig. 11 compares the short-time part of the Brownian correlation function with the short-time cumulant expansion which is correct up to $O(t^2)$. Even for very small time there are considerable deviations from the linear law.

Figure 12 shows the normalized density autocorrelation function $\Phi(k,t)$ for a smaller wave number, namely $k=4.9/a$ (the reason for this particular choice of k will become clear later), while the corresponding susceptibili-

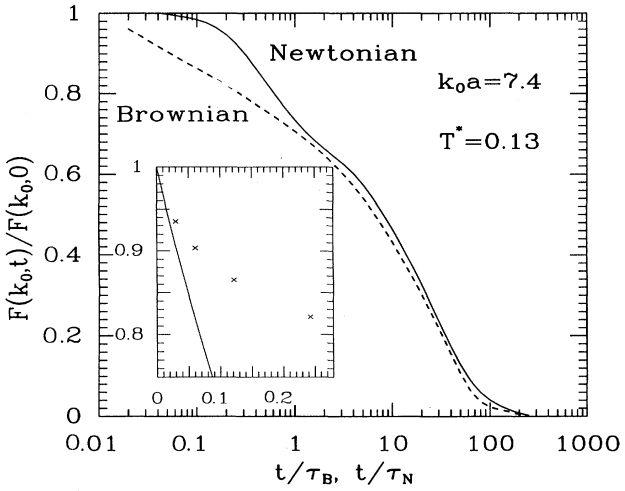

FIG. 11. Normalized density autocorrelation function $F(k,t)/S(k)$ vs reduced time ($t^*=t/\tau_N$ or t/τ_B), on a logarithmic scale for $k=k_0=7.4/a$ and $T^*=0.13$. Solid curve, Newtonian dynamics; dashed curve, Brownian dynamics. The inset shows the short-time part (on a linear scale) of the Brownian correlation function (crosses) together with the short-time approximation $\exp[-D_0k^2t/S(k_0)]$.

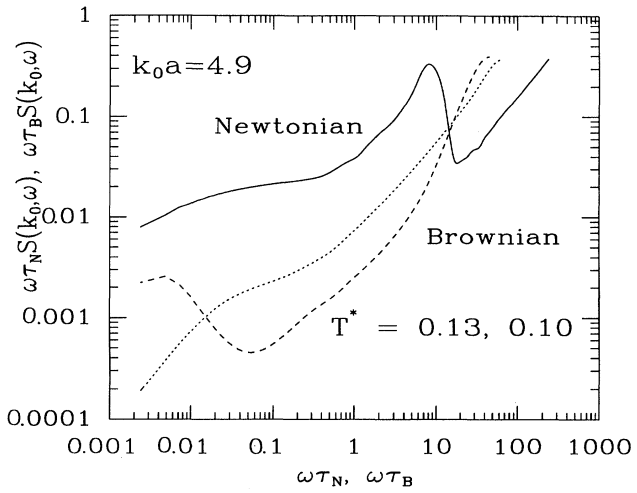

FIG. 13. Imaginary part of the density response function, $\chi''_S(k,\omega)=\omega\tau S_S(k,\omega)$, vs reduced frequency $\omega\tau$ (on a logarithmic scale) corresponding to the results of Fig. 12.

ties $\chi''(k,\omega)$ are plotted in Fig. 13. Whereas the Brownian correlation decays monotonously, its Newtonian counterpart exhibits marked oscillations, which give rise to a well-defined longitudinal phonon resonance in the susceptibility spectrum; the corresponding resonance is overdamped by solvent friction in the Brownian case, as expected. The low-frequency α resonance is less well resolved, particularly with Newtonian dynamics, compared to the situation at larger wave number shown in Fig. 10. The β resonance is again absent in the Brownian case, while it is masked by the phonon resonance in the Newtonian case, where it is only apparent as a poorly resolved shoulder on the low-frequency side of that peak. Below the glass transition temperature, the α peak in the Brownian spectrum is seen to be shifted considerably to lower frequencies, still without any trace of a β resonance.

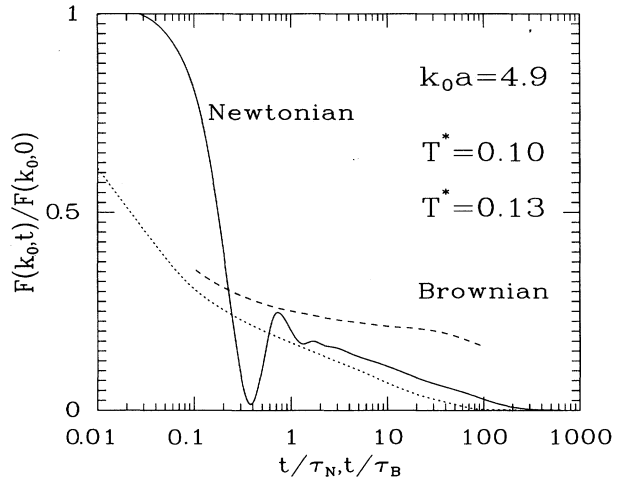

FIG. 12. Same as in Fig. 11 (without the inset), but for a smaller wave number ($k_0a=4.9$). Additionally the Brownian curve for $T^*=0.10$ is shown (long-dashed line).

An "ideal" kinetic glass transition as predicted by mode-coupling theory [5] is characterized by structural arrest, whereby the density autocorrelation function exhibits nonergodic behavior at and below a glass transition temperature T_0: instead of decaying to zero at long times, $\Phi(k,t)$ tends to a nonzero value $\xi_k=\Phi(k,t=\infty)$, frequently referred to as the Edwards-Anderson order parameter [18]; in other words, α relaxation is expected to be suppressed for $T\leq T_0$. In fact, such a sharp transition is always smeared out by decay channels, like activated processes, which restore ergodicity (and hence α relaxation) at sufficinetly long times. However, ξ_k may conventionally be defined as the plateau value of the normalized function $\Phi(k,t)$; such an identification is relatively unambiguous for Newtonian dynamics, where the correlation function exhibits a nearly horizontal portion between the β- and α-relaxation regimes, but less clear-cut in the Brownian case. The resulting order parameters ξ_k^N and ξ_k^B are plotted versus k in Fig. 14, for a temperature slightly below the transition ($T=0.115$). The frozen structure is seen to exhibit a strong, oscillatory k dependence, featuring a sharp peak at the position of the maximum of the structure factor $S(k)$ ($k\simeq k_0=7.4/a$), preceded by a pronounced minimum at $k\simeq 4.9/a$; this is precisely the wave number for which we explored the phonon resonance (cf. Figs. 12 and 13).

The k dependence of ξ_k shown in Fig. 14 is rather similar to that obtained for the binary-alloy model, both by MD simulations [10] and from mode-coupling theory

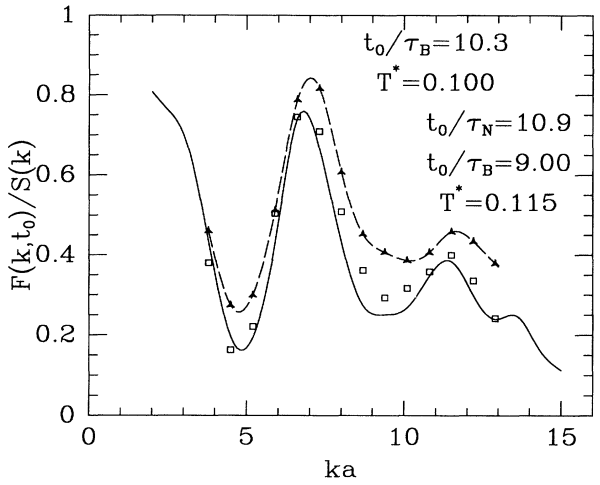

FIG. 14. Edwards-Anderson order parameter, conventionally defined as $\xi_k = F(k,t)/S(k)$ vs reduced wave number ka, for $t^* = t_0^* = 10.9$ (Newtonian dynamics, solid curve) and $t^* = t_0^* = 7.28$ (Brownian dynamics, squares). The temperature is $T^* = 0.115$. Additionally, the results for $T^* = 0.10$ are shown (triangles) in the Brownian case. The dashed line is a guide for the eye.

[19]; it also resembles the very recent dynamic-light-scattering data of van Megen and Pusey [4] for suspensions of hard-sphere-like colloidal particles. It is noteworthy that the results shown in Fig. 14 obtained with Newtonian and Brownian dynamics are very close. This may perhaps not be too surprising, since the relaxed "broken-up" structure should not be very sensitive to the details of the dynamics, in view of the predominance of excluded volume effects which leave only restricted possibilities for spatial rearrangements. In Fig. 14, the plateau value ξ_k^B is also shown for a temperature significantly below the kinetic glass transition where it is shifted to higher values in accordance with recent measurements [4] and mode-coupling theory.

VII. DISCUSSION

The main conclusion to be drawn from the present MD and BD simulations of a simple model for colloidal suspensions is the qualitative difference in the time dependence of structural relaxation, between systems governed by Newtonian and Brownian equations of motion. In particular, while Newtonian dynamics lead to correlation functions very similar to those calculated [5,10,17] or observed [6] for atomic systems, we found no evidence for β relaxation nor for a clear-cut separation of time scales in the density autocorrelation functions based on Brownian dynamics. This observation is perhaps not so unexpected, since a straightforward memory function analysis, sketched in the Appendix, shows that contrarily to the Newtonian case, Brownian dynamics preclude any possibility of an *ideal* glass transition, as characterized by complete structural arrest. This qualitative conclusion, a direct consequence of the irreversible nature of Brownian dynamics, is quite general and independent of any specific approximation for the memory function, like the mode-coupling ansatz.

Another important result of the Brownian simulations is the clear evidence for hopping processes around and below the alleged glass transition temperature. The resulting jump diffusion is a well-known feature in atomic systems, governed by Newtonian dynamics, where it is induced by cooperative phonon processes, but it is more unexpected with Brownian dynamics, where collective motions are strongly damped by solvent friction. Activated hopping processes appear thus as the primary mechanism for α relaxation, although the detailed dynamical nature of these jumps is different in the Newtonian and Brownian cases, as illustrated by the significant difference in the Kohlrausch exponents. In the Newtonian case, the jumps are assisted by collective phonon processes, distorting the cages, whereas these same cages fluctuate in the Brownian case, due to the independent random displacements of the particles that form the cages.

It is important to note that the sharp crossover in the diffusion mechanism, from hydrodynamiclike to jump diffusion, manifest in the Van Hove functions $G_S(r,t)$ shown in Fig. 7, does not give rise to a concomitant qualitative change in the shape of the corresponding intermediate scattering function $F_S(k,t)$ calculated with Brownian dynamics. If the above-mentioned crossover is chosen as a diagnostic for the kinetic glass transition temperature T_0^B, it is apparent from Fig. 10 that a roughly horizontal plateau shows up in $F_S(k,t)$ only well below that temperature in the Brownian case, whereas the separation of time scales, characteristic of an "ideal" glass transition, is more clear-cut in the vicinity of the glass transition temperature T_0^N with Newtonian dynamics.

The remaining question is that of the relevance of our model calculations for real colloidal systems. In particular, it is of obvious interest to confront the simulation data of the present paper with the recent extensive dynamic-light-scattering measurements of structural relaxation in concentrated colloidal suspensions by van Megen and Pusey [4]. The latter data are for suspensions of sterically stabilized colloidal particles, which may be reasonably modeled by hard sheres [5], while we simulated a model of charge-stabilized colloidal particles interacting via the pair potentials (1). However, in the strong screening regime considered here ($\kappa = 7$), the direct interactions are harshly repulsive, so that it is not unreasonable to assume that the present system should behave like some underlying effective hard-sphere system. If the Gibbs-Bogoliubov inequality is used to map our model onto such an effective hard-sphere system [9], it is found that a glass transition temperature $T^* \simeq 0.12$ corresponds to a critical hard-sphere packing fraction $\eta \simeq 0.522$, a value relatively close to the critical packing fraction $\eta \simeq 0.565$ reported by van Megen and Pusey [4].

Direct comparison of the density autocorrelation functions plotted in Figs. 8 and 9 with the corresponding results in Ref. [4] shows that the general behavior of the two sets of data is consistent. We believe that the kinetic glass transition, as characterized by the above-mentioned

crossover of diffusion regimes, takes place *before* the density autocorrelation function develops a marked horizontal portion, contrarily to the Newtonian case. This means that the critical packing fraction in the experiments may be lower than the value $\eta \simeq 0.565$, estimated by van Megen and Pusey [4] from the onset of a horizontal plateau. This leads to a closer agreement with the effective packing fraction derived from our glass-transition temperature and is consistent with estimates from hard-sphere computer simulation [20], mode-coupling [21] and density-functional theories [22]. Another encouraging feature is that the Kohlrausch exponent in Eq. (20), characterizing the final α relaxation, is significantly closer to 1 for Brownian dynamics as compared to the Newtonian case, in qualitative agreement with the value $\nu \simeq 0.9$ reported in Ref. [4].

As already stressed earlier, our BD simulations account only for part of the solvent effects, namely, the friction exerted on each individual colloidal particle, but ignore solvent-mediated hydrodynamic interactions between these particles. This drastic simplification is unavoidable if the primary objective is the exploration of slow relaxation processes. Much more theoretical and numerical work is required to obtain a more realistic description of the dynamics in concentrated colloidal suspensions [23]. Intuitively, one may expect that an inclusion of lubrication forces leads to a further hindering of structural relaxation. The above-mentioned limitation of our model, however, does not affect our main conclusion, namely that the long-time behavior of structural relaxation is very sensitive to the mathematical nature of the underlying equations of motion.

ACKNOWLEDGMENTS

The authors are grateful to Wolfgang Götze and Peter Pusey for making available Refs. [5] and [4] before publication. One of us (H. L.) acknowledges financial support by "Deutsche Forschungsgemeinschaft." Laboratoire de Physique is "Unité Associée au Centre National de la Recherche Scientifique No. 1325."

APPENDIX

In this appendix we briefly consider the possibility of structural arrest, as signaled by a nonzero value of the $t \to \infty$ limit of the normalized density autocorrelation function, $\xi_k = \Phi(k, t=\infty)$, within the memory function formalism. The Mori-Zwanzig projection operator technique, which is very familiar for atomic or molecular systems governed by Newtonian dynamics and the Liouville evolution operator (10), is also applicable to Brownian dynamics and the Smoluchowski operator (11) [24]. The formalism is applied here to the two-component dynamical variable $\underline{A}_{\mathbf{k}} = \{A_{\mathbf{k}1}, A_{\mathbf{k}2}\}$, made up of the microscopic density (18)

$$A_{\mathbf{k}1}(t) = \rho_{\mathbf{k}}(t) \tag{A1}$$

and its derivative, the longitudinal current

$$A_{\mathbf{k}2} = j^l_{\mathbf{k}}(t) = -\frac{i}{k}\dot{\rho}_{\mathbf{k}}(t) \ . \tag{A2}$$

The dot denotes a time derivative; according to Eqs. (10) and (11):

$$A_{\mathbf{k}2} = \begin{cases} -\dfrac{i}{k}\mathcal{L}\rho_{\mathbf{k}}(t) \ \text{(Newtonian dynamics)} & \text{(A3a)} \\ -\dfrac{i}{k}\tilde{\mathcal{O}}\rho_{\mathbf{k}}(t) \ \text{(Brownian dynamics)} \ . & \text{(A3b)} \end{cases}$$

The choice of $\underline{A}$ is the one usually made in the mode-coupling investigations of the glass transition in atomic systems [5]. In the case of Newtonian dynamics, $\rho_{\mathbf{k}}$ and $j^l_{\mathbf{k}}$ are conserved variables in the $k \to 0$ limit, corresponding to the conservation of total mass and (longitudinal) momentum, whereas in the Brownian case, only $\rho_{\mathbf{k}}$ is conserved, but not $j^l_{\mathbf{k}}$, due to the frictional exchange of momentum with the solvent. Note that in view of Eqs. (10), (11), and (A3), the longitudinal current $j^l_{\mathbf{k}}$ is a function of particle positions and momenta in the Newtonian case, but only of particle positions within Brownian dynamics.

A straightforward application of the projection operator formalism leads to the familiar memory function equation (see, e.g., [25]), written in Laplace space

$$[-iz - i\underline{\Omega}(k) + \underline{\tilde{M}}(k,z)]\underline{\tilde{C}}(k,z) = \underline{C}(k,0) \ , \tag{A4}$$

where $\underline{\tilde{C}}$ is the Laplace transform of the 2×2 correlation function matrix

$$\underline{C}(k,t) = (\underline{A}_{\mathbf{k}}(t), \underline{A}_{\mathbf{k}}(0)) \ , \tag{A5}$$

$(\ ,\ )$ denoting the usual scalar product (i.e., the phase-space average) in the Hilbert space of dynamical variables; $i\underline{\Omega}(k)$ is the "frequency matrix:"

$$i\underline{\Omega}(k) = (\dot{\underline{A}}_{\mathbf{k}}, \underline{A}_{\mathbf{k}})(\underline{A}_{\mathbf{k}}, \underline{A}_{\mathbf{k}})^{-1} \ . \tag{A6}$$

The memory function matrix $\underline{M}(k,t)$ is defined, as usual, as the autocorrelation function of the random force. The reversible (irreversible) nature of Newtonian and Brownian dynamics leads to very different forms of the $i\underline{\Omega}$ and $\underline{M}$ matrices:

$$i\underline{\Omega} = \begin{bmatrix} 0 & ik \\ \dfrac{ikv_0^2}{S(k)} & 0 \end{bmatrix} \ , \qquad \underline{M} = \begin{bmatrix} 0 & 0 \\ 0 & m(k,t) \end{bmatrix} \ \text{(Newtonian)} \ , \tag{A7a}$$

$$i\underline{\Omega} = \begin{bmatrix} 0 & ik \\ i\Omega_{21}(k) & i\Omega_{22}(k) \end{bmatrix} \ , \qquad \underline{M} = \begin{bmatrix} 0 & 0 \\ -\dfrac{iD_0 k m(k,t)}{\Delta(k)} & \dfrac{S(k)}{\Delta(k)} m(k,t) \end{bmatrix} \ \text{(Brownian)} \ , \tag{A7b}$$

where $v_0^2 = k_B T/m$, $\Delta(k) = (1/k^2)S(k)\ddot{F}(k,t=0) - D_0^2 k^2$ and $\Omega_{21}(k)$, $\Omega_{22}(k)$ are k-dependent quantities which may be calculated from a knowledge of the static pair and triplet correlation functions. The key point is that $i\Omega_{22}(k)$ and $M_{12}(k,t)$ are nonzero in the Brownian case. The resulting equations of motion for the normalized

density autocorrelation function $\Phi(k,t)=F(k,t)/S(k)$ read

$$\ddot{\Phi}(k,t)+\Omega_0^2\Phi(k,t)+\frac{1}{v_0^2}\int_0^t m(k,t-t')\dot{\Phi}(k,t')dt'=0 \quad \text{(Newtonian)}, \tag{A8a}$$

where $\Omega_0^2=v_0^2k^2/S(k)$, and

$$\ddot{\Phi}(k,t)+J_1\dot{\Phi}(k,t)+\Omega_0^2\Phi(k,t)+\int_0^t M(k,t-t')[\dot{\Phi}(k,t')+J_0\Phi(k,t')]dt'=0 \quad \text{(Brownian)}, \tag{A8b}$$

where now $\Omega_0^2=\Omega_{21}(k)k$, $M(k,t)=[S(k)/\Delta(k)]m(k,t)$, and the real "friction" coefficients (not present in the Newtonian case) are $J_0=D_0k^2/S(k)$ and $J_1=i\Omega_{22}(k)$. The dissipative terms in (A8b) explain the overdamping of the collective phonon modes.

Returning to the Laplace transforms, (A8a) and (A8b) can be solved in the form

$$\tilde{\Phi}(k,z)=\frac{\tilde{M}(k,z)-iz}{-z^2-iz\tilde{M}(k,z)+\Omega_0^2} \quad \text{(Newtonian)}, \tag{A9a}$$

$$\tilde{\Phi}(k,z)=\frac{\tilde{M}(k,z)-iz-(J_0+J_1)}{-z^2+iz\dot{J}_1-(iz-J_0)\tilde{M}(k,z)+\Omega_0^2} \quad \text{(Brownian)}, \tag{A9b}$$

where $\tilde{M}=\tilde{m}/v_0^2$ in the Newtonian case and $\tilde{M}=S(k)\tilde{m}/\Delta(k)$ in the Brownian case. Nonergodic behavior is characterized by a nonzero value ξ_k of the $t\to\infty$ limit of $\Phi(k,t)$, and hence by a $1/z$ pole of $\tilde{\Phi}(k,z)$ for $z\to 0$. It is easy to see that the existence of such a pole is consistent with Eq. (A9a); the residue ξ_k is related to the residue M_k of a similar pole in $\tilde{M}(k,z)$ according to

$$\xi_k=\frac{M_k}{\Omega_0^2+M_k}, \tag{A10a}$$

so that a nonergodic behavior of the memory function induces a finite ξ_k and vice versa.

In the case of Brownian dynamics, on the other hand

$$\tilde{\Phi}(k,z\to 0)=\frac{iM_k+O(z)}{iJ_0M_k+O(z)}, \tag{A10b}$$

which shows that $\tilde{\Phi}$ is regular ($\xi_k=0$), even if the memory function has a $1/z$ pole (i.e., $M_k\neq 0$), except in the limit $D_0\to 0$ (and hence $J_0\to 0$), which would lead back to Newtonian dynamics. Thus it appears that Brownian dynamics, characterized by the Smoluchowski evolution operator (11), cannot lead to an ideal glass transition. This conclusion is quite general, and independent of the mode-coupling assumption for the memory function.

An alternative description of solvent effects could be based on Fokker-Planck dynamics, where the velocities of the colloidal particles are explicitly included. This approach would be well adapted to the description of ionic solutions [26], but seems inappropriate in the present case, due to the complete separation of time scales.

---

*Permanent address: Sektion Physik der Universität München, Theresienstrasse 37, D-8000 München 2, Germany.

[1] For a recent review, see P. N. Pusey, in *Liquids, Freezing and the Glass Transition,* edited by J. P. Hansen, D. Levesque, and J. Zinn-Justin (North-Holland, Amsterdam, in press).

[2] P. Pieranski, Contemp. Phys. **24**, 25 (1983).

[3] P. N. Pusey and W. van Megen, Nature (London) **320**, 340 (1986).

[4] P. N. Pusey and W. van Megen, Phys. Rev. Lett. **59**, 2083 (1987); Ber. Bunsenges. Phys. Chem. **94**, 225 (1990); W. van Megen and P. N. Pusey, Phys. Rev. A **43**, 5429 (1991); W. van Megen (unpublished).

[5] W. Götze and L. Sjögren, Phys. Rev. A **43**, 5442 (1991); for a recent review, see W. Götze, in *Liquids, Freezing and the Glass Transition,* edited by J. P. Hansen, D. Levesque, and J. Zinn-Justin (North-Holland, Amsterdam, in press).

[6] F. Mezei, W. Knaak, and B. Farago, Phys. Rev. Lett. **58**, 571 (1987); W. Knaak, F. Mezei, and B. Farago, Europhys. Lett. **7**, 529 (1988).

[7] M. P. Allen and D. J. Tildesley, *Computer Simulation of Liquids* (Clarendon, Oxford 1987).

[8] D. L. Ermak, J. Chem. Phys. **62**, 4189 (1975); **62**, 4197 (1975).

[9] H. Löwen, J. N. Roux, and J. P. Hansen, J. Phys. Cond. Matt. **3**, 997 (1991).

[10] J. N. Roux, J. L. Barrat and J. P. Hansen, J. Phys. Condens. Matter **1**, 7171 (1989); J. L. Barrat, J. N. Roux, and J. P. Hansen, Chem. Phys. **149**, 197 (1990).

[11] M. O. Robbins, K. Kremer, and G. S. Grest, J. Chem. Phys. **88**, 3286 (1988).

[12] J. L. Barrat and J. P. Hansen, J. Phys. **47**, 1547 (1986); P. N. Pusey, J. Phys. **48**, 709 (1987).

[13] N. Pistoor and K. Kremer, in *Dynamics of Disordered Materials,* edited by D. Richter, A. J. Dianoux, W. Petry, and J. Teixera (Springer, Berlin, 1989); R. O. Rosenberg and D. Thirumalai, Phys. Rev. A **36**, 5690 (1987).

[14] K. Gaylor, I. Snook, and W. van Megen, J. Chem. Phys. **75**, 1682 (1981).

[15] M. Dzugutov and U. Dahlborg, J. Non-Cryst. Solids (to be published).

[16] H. Migayawa, Y. Hiwatari, B. Bernu, and J. P. Hansen, J. Chem. Phys. **88**, 3879 (1988); Y. Hiwatari and H. Migayawa, J. Non-Cryst. Solids **118**, 862 (1989).

[17] G. F. Signorini, J. L. Barrat, and M. L. Klein, J. Chem. Phys. **92**, 1294 (1990).

[18] S. F. Edwards and P. W. Anderson, J. Phys. F **5**, 965 (1975).

[19] J. L. Barrat and A. Latz, J. Phys. Condens. Matter **2**, 4289 (1990).

[20] L. V. Woodcock, C. A. Angell, Phys. Rev. Lett. **47**, 1129 (1981).

[21] J. L. Barrat, W. Götze, and A. Latz, J. Phys. Condens. Matter **1**, 7163 (1989).
[22] H. Löwen, J. Phys. Condens. Matter **2**, 8477 (1990).
[23] W. van Megen and I. Snook, J. Chem. Phys. **88**, 1185 (1988).
[24] P. G. Wolynes and J. M. Deutch, J. Chem. Phys. **67**, 733 (1977); B. J. Ackerson, *ibid.* **69**, 684 (1978); W. Hess and R. Klein, Adv. Phys. **32**, 173 (1983).
[25] J. P. Hansen and I. MacDonald *Theory of Simple Liquids,* 2nd ed. (Academic, London, 1986).
[26] P. Turq, F. Lantelme, and H. L. Friedman, J. Chem. Phys. **66**, 3039 (1977).